



Cite this: DOI: 10.1039/c7gc03163g

Received 20th October 2017,
Accepted 9th January 2018

DOI: 10.1039/c7gc03163g

rsc.li/greenchem

Sono-transformation of tannic acid into biofunctional ellagic acid micro/nanocrystals with distinct morphologies†

Sukhvir Kaur Bhangu,^a Ritu Singla,^a Enrico Colombo,^a Muthupandian Ashokkumar^b *^a and Francesca Cavalieri^b *^{b,c}

A sustainable, reagent-less and one-pot ultrasonic methodology has been developed to transform amorphous tannic acid into regularly shaped crystalline ellagic acid particles. Multiple and consecutive reactions have been performed on tannic acid, in aqueous solution without the addition of any external reagent. The size, morphology and bio-activity of ellagic acid micro-nanocrystals can be finely tuned by choosing appropriate ultrasonic parameters.

Acoustic cavitation in aqueous solutions results in the generation of a reactive green processing environment enabling a number of reactions without the addition of any external reagents. Extremely high local temperatures and pressures, oxidizing and reducing agents and physical effects (microjets, turbulence, shear forces, *etc.*) are generated by acoustic cavitation, which may exert synergistic effects. High and low frequency ultrasound has been employed in materials synthesis, polymerization, degradation of organic and inorganic pollutants, wastewater treatment, crystallisation, and microcapsule synthesis encapsulating food and cosmetic ingredients.^{1–4}

Recently, we have demonstrated a new concept that cavitation bubbles generated by high frequency ultrasound in the range of 0.35–1 MHz can act as catalytic binding sites for the radical mediated C–C coupling of phenolic moieties.^{5,6} Simple phenolic molecules such as tyrosine and phenol were coupled by a C–C linkage to form oligomeric bio-functional phenolic systems, which are not obtained with other radical sources (such as Fenton's reaction).

Herein, we show that cavitation bubbles are simple micro-reactors with reactive surfaces to perform one-pot multiple reactions on complex organic molecules, namely (i) hydrolysis of an ester linkage, (ii) C–C coupling reactions, (iii) conden-

sation reactions and (iv) crystallisation of the product into regularly shaped particles. To our knowledge, multiple and consecutive reactions induced by acoustic cavitation have never been reported before.

As a proof of concept, we have developed a sustainable, reagent-less and cost effective synthetic methodology to transform amorphous tannic acid into regularly shaped crystalline ellagic acid particles, with tunable morphologies and functionality. The size and shape of ellagic acid micro-nanocrystals can be finely tuned by choosing appropriate ultrasonic parameters such as sonication time, power and frequency. Ellagic acid powder is conventionally obtained either through the enzymatic hydrolysis oxidation of ellagitannins with tannase and decarboxylase^{7,8} or multistep organic synthesis⁹ without any control over size and shape.

Conversely, in this work we demonstrate a remarkably simple and unique green synthetic route to generate ellagic acid micro-nanocrystals. In addition, our approach should be readily extendable to other sono-responsive biomolecules.

The chemical functionalization and assembly of phenolic biomolecules such as gallotannins, ellagitannins, catechins and flavonoids have recently attracted much attention due to their potential application in different fields including sensing, imaging, drug delivery, live-cell protection, and catalysis.^{10–13} The current approaches for the manipulation of phenol moieties into the desired nanoarchitectures require the formation of catechol–metal coordination complexes or oxidative coupling reactions catalyzed by metals or enzymes.¹⁴ The biomolecule obtained in this study, ellagic acid (EA), is of particular interest in the biomaterials area because *in vitro* and *in vivo* studies have shown that EA can significantly inhibit cancer formation in the colon, oesophagus, liver, lung, tongue and skin and the infection of human T-cell lymphotropic virus type-1-carrying MT-4 cells by human immunodeficiency virus (HIV).^{7,15}

The direct sono-transformation of tannic acid into ellagic acid micro-nanoparticles is a versatile method for the engineering of ellagic acid-based biomaterials with tailored structural and functional properties.

^aSchool of Chemistry, The University of Melbourne, VIC 3010, Australia.

E-mail: masho@unimelb.edu.au

^bDepartment of Chemical and Biomolecular Engineering, The University of Melbourne, VIC 3010, Australia. E-mail: francesca.cavalieri@unimelb.edu.au

^cDipartimento di Scienze e Tecnologie Chimiche, Università di Roma "Tor Vergata", via della ricerca scientifica 1, 00133 Rome, Italy

† Electronic supplementary information (ESI) available. See DOI: 10.1039/c7gc03163g

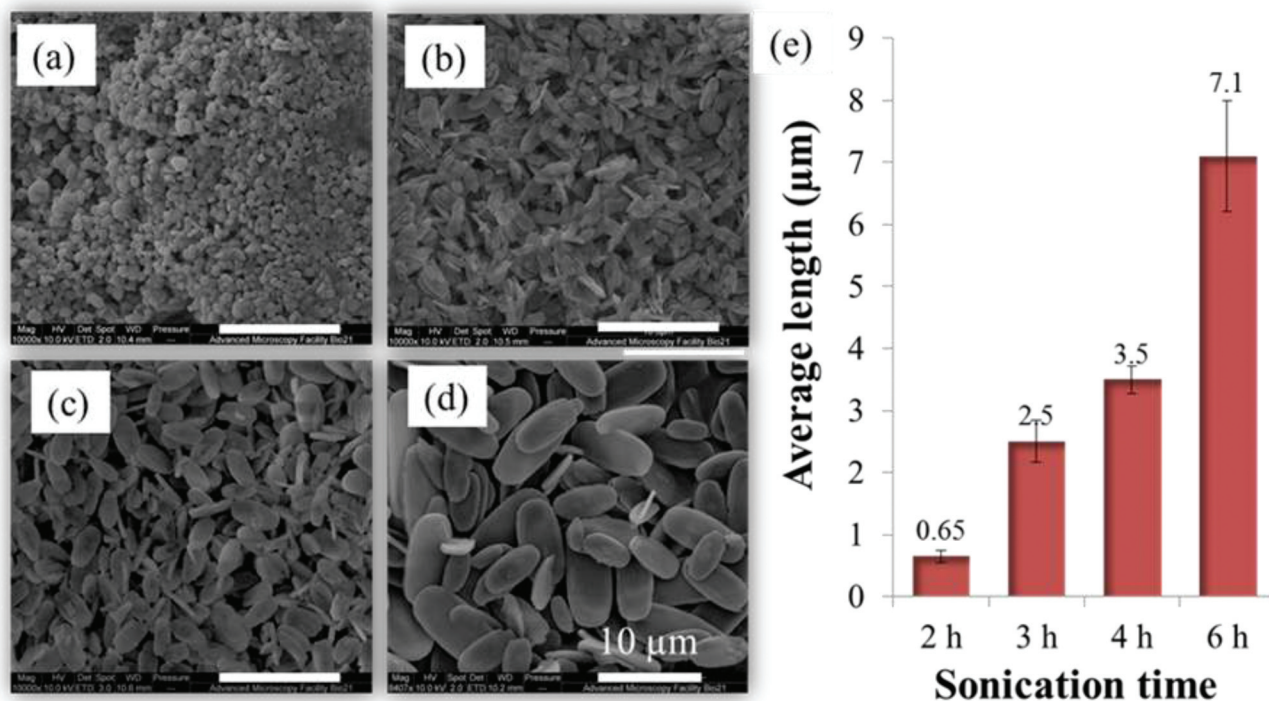


Fig. 1 The effect of sonication time on the TAS particles obtained. (a) 2 h, (b) 3 h, (c) 4 h, and (d) 6 h; (e) average length of the particles as a function of sonication time (scale bar = 10 μm). Samples were sonicated at 355 kHz and 5.5 W cm⁻³.

Tannic acid is a biomass belonging to the category of hydrolysable tannins with a multiple number of gallic acid and galloyl units attached to the central sugar core which is mostly D-glucopyranose.^{16,17} The aim of the study was to explore the chemical transformation of tannic acid induced by ultrasound. The sonication of an aqueous solution of tannic acid at 355 kHz and 5.5 W cm⁻³ was carried out at pH 7 for up to six hours. Surprisingly, we discovered that the sonicated tannic acid undertook a more complex modification pathway. We observed the formation of nano-micrometer sized crystalline particles hereafter referred to as TAS particles. The SEM images of the TAS particles obtained after different sonication times are shown in Fig. 1a–d. It can be seen that the size, shape and morphology of the crystals depends on the sonication time. Nanoparticles with a discoidal shape turned into a flat ellipsoidal shape growing in size. The graph shown in Fig. 1e illustrates that the average length of particles increased from 650 nm to 7 μm when the sonication time was increased from 2 h to 6 h.

We sought to investigate the chemical composition and the mechanism of the formation of the obtained particles. In order to gain insight into the composition of TAS particles mass spectrometry, spectroscopy, chromatography and NMR analysis were conducted. The electrospray mass spectrometry (ESMS) and MALDI-TOF data (Fig. S1a, ESI[†]) acquired after the dissolution of the TAS particles in Milli-Q water have shown the presence of a major peak at *m/z* 301 that could be assigned to ellagic acid (see Fig. 2 for the structure),

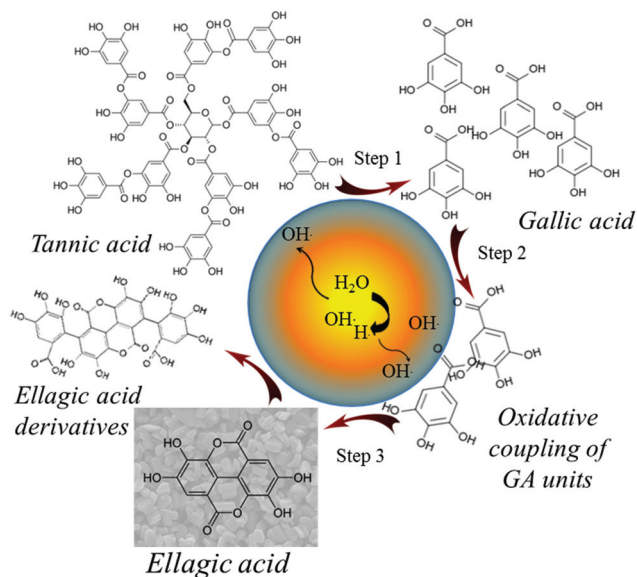


Fig. 2 Schematic of the proposed mechanism for the ultrasonic transformation of TA to ellagic acid. The core of cavitation bubbles generating high temperatures leading to the homolysis of the water molecule to H[•] and OH[•], step 1 showing the hydrolysis of tannic acid to gallic acid, step 2 the oxidative coupling of gallic acid units at the bubble surface to form a dimer and step 3 where the dimer spontaneously lactonized to form EA and its derivatives.

accompanied by some small peaks ascribed to higher molecular weight species (Fig. S1a and b, ESI†). The sono-transformation of tannic into ellagic acid was further confirmed by HPLC (Fig. S1, ESI†), absorption spectroscopy, ^1H and ^{13}C NMR spectroscopy (Fig. S2–S5, ESI† respectively) and PXRD analyses.

In particular the X-ray diffraction patterns indicate that commercial tannic acid is amorphous, which is consistent with the literature,¹⁸ whereas the TAS particles are crystalline (Fig. S6, ESI†). The X-ray diffraction pattern of the TAS particles was identical to the commercial ellagic acid,¹⁹ for example, peaks at 2θ values of 17.9° , 21.4° , 24.8° , 26.7° and 28.5° , indicating the crystalline nature of the particles.²⁰ However, some additional peaks were also observed. Overall our data suggest that high frequency sonication provides a simple one-step approach for the synthesis of crystalline ellagic acid particles from tannic acid with different shapes and sizes. Fig. 2 shows the possible mechanism involved in the formation of ellagic acid from TA. It is well known that cavitation bubbles driven by high frequency ultrasound can give rise to physical effects such as shear forces, turbulence, microjets, *etc.* and chemical effects such as the generation of radicals due to the homolysis of water to H^\cdot to OH^\cdot (Fig. 2). The recombination of 2 OH^\cdot would lead to the formation of H_2O_2 .^{1,3} The combination of all these effects can play a significant role in inducing different chemical reactions. TA is composed of a multiple number of galloyl units and shear stress and radicals generated by cavitation induces the hydrolysis of galloyl moieties (step 1) without the use of any acid or base catalyst. Subsequently, two gallic acid units undergo catalytic oxidative coupling through a C–C linkage to form a dimer at the bubble–solution interface (step 2) as observed in our previous studies.^{5,6} The spontaneous lactonization likely occurs in the bulk phase to form EA (step 3).

Ellagic acid can further react with gallic acid molecules on the surface of cavitation bubbles to form derivatives by C–C oxidative coupling mediated by OH^\cdot radicals. Finally, the ultrasound assisted assembly and crystallisation of ellagic acid completes the series of reactions triggered by ultrasound.

Ultrasound assisted crystallisation has been reported in the literature and it was suggested that the ultrasonic parameters can be used to control size distribution, average crystal size and type of polymorph obtained.^{21–23} Particularly, crystal size can be controlled by two cavitation effects, the generation of shock waves by acoustic cavitation which increases the nucleation rate and microturbulence that can direct the subsequent growth of the crystals.²² Interestingly, different crystal morphology was observed at different sonication times. After two hours of sonication, the EA concentration reaches the supersaturation condition, forming submicron particles (Fig. 1a). Subsequently the ultrasonically generated EA, with increasing sonication time, contributes to the particle growth up to 7 micrometers (Fig. 1d). It is worth noting that the use of OH^\cdot radicals generated from hydrogen peroxide sources, such as Fenton's reagents, didn't result in the formation of fluorescent and regularly shaped particles. This suggests that the simultaneous presence of OH^\cdot radicals and a reactive cavitation

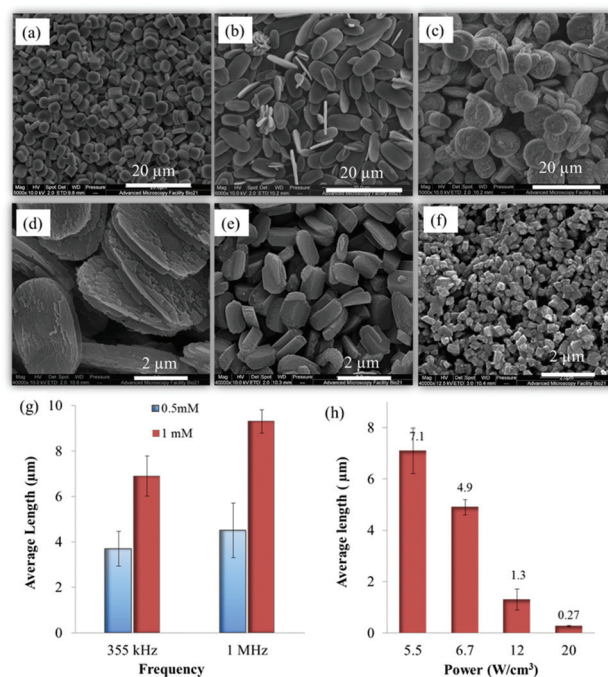


Fig. 3 SEM images of the TAS particles obtained using different TA concentrations and ultrasonic parameters: (a) TA 0.5 mM at 355 kHz and 5.5 W cm^{-3} , (b) TA 1 mM at 355 kHz and 5.5 W cm^{-3} , (c) TA 1 mM at 1 MHz and 5.5 W cm^{-3} ; (d) SEM image of the TAS particles at 355 kHz and 6.7 W cm^{-3} , (e) SEM image of the TAS particles at 355 kHz and 12 W cm^{-3} , (f) SEM image of the TAS particles at 355 kHz and 20 W cm^{-3} ; (g) the graph provides the average length of the TAS particles at different concentrations of TA as a function of ultrasonic frequency and (h) average length of the TAS particles as a function of ultrasonic power.

bubble interface are necessary for the coupling of gallic acid molecules.

In order to gain further insight into the effect of ultrasonic parameters on EA particle morphologies, further experiments were carried out. Fig. 3 shows the SEM images of the TAS particles obtained as a function of different ultrasonic frequencies (355 kHz and 1 MHz), initial concentrations of TA (0.5 mM and 1 mM) and ultrasonic powers (5.5, 6.7, 12, and 20 W cm^{-3}). Micro-nanoparticles with different morphologies were obtained including small and large discoidal shape particles, flat ellipsoidal particles and brick-like particles. These images suggest that the morphology of the TAS particles is affected significantly by the experimental parameters. When the initial concentration of TA was increased from 0.5 mM (Fig. 3a) to 1 mM (Fig. 3b), the size of the particles increased from 3.7 to 7 μm at 355 kHz. Also, when the ultrasonic frequency was switched from 355 kHz (Fig. 3b) to 1 MHz (Fig. 3c) at 1 mM concentration of TA, changes in the morphology, *viz.*, size (from 7 to 9.5 microns) as well as the aspect ratio, *i.e.*, the length to width ratio (from 1.8 to 1.1) of the crystals, were observed.

Similarly, the effect of ultrasonic power was studied on the morphology and the size of the TAS crystals. Fig. 3d, e and f represent the SEM images of the particles obtained when TA

solution was sonicated for 5 hours at 6.7 W cm^{-3} , 12 W cm^{-3} and 20 W cm^{-3} , respectively. The results showed that when the power was increased from 5 W cm^{-3} to 20 W cm^{-3} , the crystal size reduced from 7 microns to 200–350 nm (Fig. 3h). Fig. 3g summarises how the average length of the TAS crystals changed with changes in the frequency and TA concentration. Also, the yield of EA produced varied from 40 to 70% when the power was increased from 5.5 W cm^{-3} to 20 W cm^{-3} .

Fig. 4 shows a schematic to explain how the morphology, size and aspect ratio of the TAS particles are affected by various parameters such as sonication time, concentration of TA, ultrasonic power and frequency. As crystal size and size distribution are influenced by the population and growth rate of the nuclei, a rise in the number of nuclei formed (nucleation rate) would lead to a reduction in the amount of the solute available for the growth of individual crystals leading to small sized crystals.^{22,23}

With an increase in the ultrasonic frequency from 355 kHz to 1 MHz, a decrease in the number of OH^\cdot radicals produced and shear forces has been reported.^{1,3} OH^\cdot radicals are required for the oxidative coupling reaction; therefore, at a higher frequency the amount of EA generated would decrease resulting in the decrease in the local supersaturation and nucleation rate; thus an increase in the crystal size and aspect ratio is observed (Fig. 3b and c).

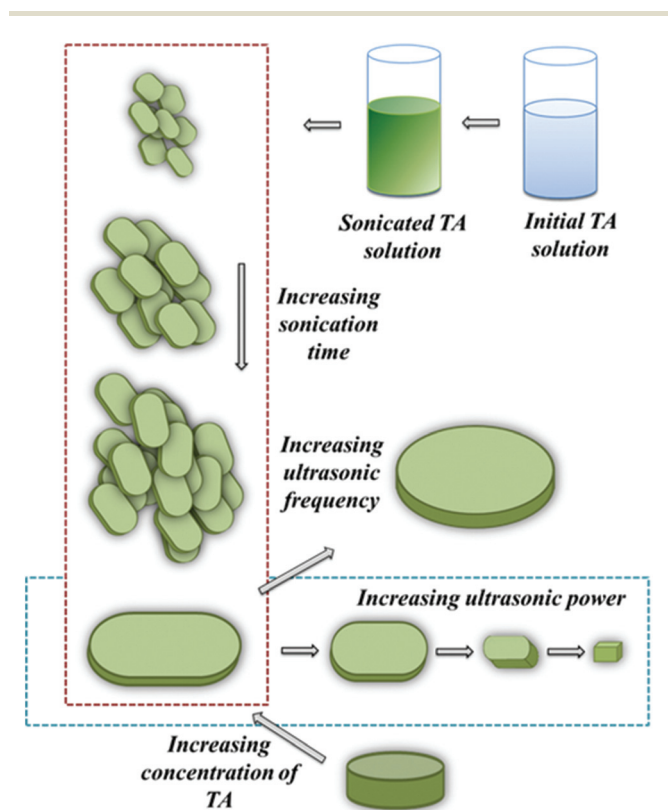


Fig. 4 Schematic illustration of the effect of sonication time, frequency, power and concentration of TA on the morphology and size of the TAS particles.

Similarly, ultrasonic power can be also used to tune the size of the particles (Fig. 3d–f). The crystal size decreases with increasing power due to the enhanced physical effects and chemical effects. Peculiarly, increased shear forces, turbulence and shock waves as well as the number of radicals (required for the oxidative coupling reaction) can significantly improve the local supersaturation resulting in higher nucleation rates and smaller crystal sizes.^{21–23} Hence, the decrease in the crystal size is observed with the upsurge of ultrasonic power.

The aspect ratio of microparticles is dictated by the concentration of ultrasonically produced EA. EA assembles into discoidal shaped particles at a higher frequency (Fig. 3c) when the rate of generation of OH^\cdot radicals is low and also at low concentrations of TA (Fig. 3a), consequently, decreasing the concentration of EA. However, at a higher concentration of EA, microparticles preferentially form ellipsoidal crystals.

The optical properties of the TAS particles were investigated by fluorescence spectroscopy and microscopy. Fig. 5a represents the fluorescence emission spectra of the TAS particles at different excitation wavelengths. It can be observed that λ_{max} is around 440 nm when excited at 360 nm. The observed spectroscopic properties were similar to those of pure EA (Fig. S7, ESI†). The dependence of the emission wavelength on the excitation wavelength indicates the presence of multiple other oli-

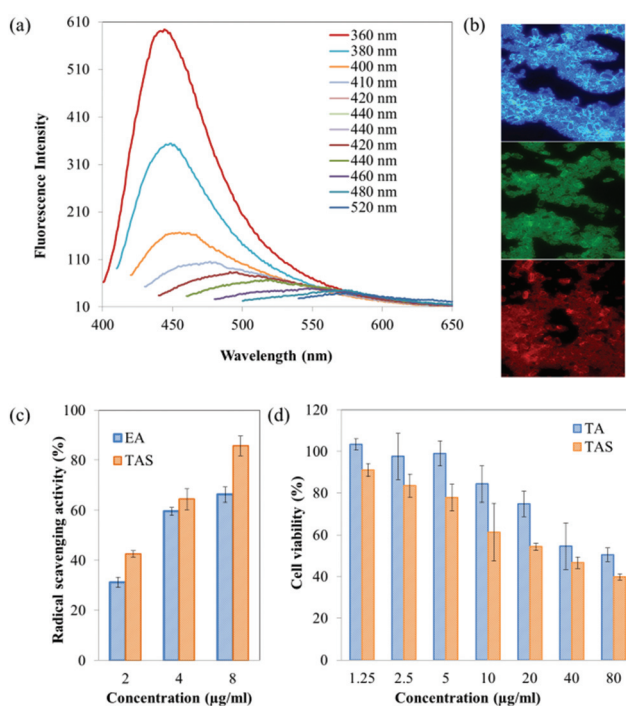


Fig. 5 (a) Fluorescence emission spectra of 1 mM TA solution sonicated at 355 kHz and 5.5 W cm^{-3} recorded at different excitation wavelengths, (b) fluorescence microscopy images of the TAS particles showing blue, green and red emission. (c) DPPH radical scavenging activity of TA and EA particles as a function of concentrations after 3 min incubation time, (d) cytotoxicity of TA and TAS as a function of the concentration after 24 h incubation at 37°C with MDA-MB-231 cells.

gomic species along with the formation of EA, in agreement with previous results. The fluorescence of the TAS particles was confirmed by fluorescence microscopy where blue, green and red emissions (Fig. 5b) were observed.

To demonstrate the functional properties of the TA and TAS particles, further studies were performed. The thermal stability study of the TA and TAS particles was performed by thermogravimetric analysis. Fig. S8, ESI† shows that the TAS particles are also more thermostable compared to tannic acid. The ζ -potentials of the TAS particles were measured to be around $-56 \text{ mV} \pm 11 \text{ mV}$ in deionized water. This indicates that the surface of the particles is negatively charged most likely due to the presence of acidic phenoxy groups and the ζ -potential of the TAS particles is in the range for the colloidal stability of the particles. Hence, the TAS particles did not aggregate in aqueous solution.

The antioxidant properties of TAS and EA were studied and compared using a DPPH assay. Fig. 5c shows the percentage radical scavenging activity of the TAS and EA particles as a function of concentration after 3 min incubation. Firstly, it was observed that the activity increased as a function of TAS and EA concentrations. Secondly, it was also observed that TAS nanoparticles had a better radical scavenging activity than EA at all the concentrations. Polyphenolic molecules have the capacity to prevent DNA and protein damage as they can scavenge the OH radicals, peroxy radicals and nitrogen reactive species²⁴ due to the high degree of hydroxylation. These results confirm that the antioxidant properties of TA are improved when converted to TAS particles. The antioxidant properties can be exploited in various biomedical applications to protect the cells and biomolecules against free radicals.

Finally, the cytotoxicity and anticarcinogenic activity of the TA and TAS nanoparticles were assessed by an MTT viability assay. MDA-MB-231 breast cancer cells were incubated with TA and EA at different concentrations. Fig. 5d shows that the TAS nanoparticles have higher anticancer activity as compared to TA at all concentrations. The IC_{50} value of the TAS particles was between 20 and $10 \mu\text{g mL}^{-1}$, whereas TA has a value $>80 \mu\text{g mL}^{-1}$. The chemo-preventive properties of different polyphenols have been determined both *in vivo* and *in vitro* in the past. They exert such effects as they have the tendency to reduce proliferation by inducing apoptosis.²⁴ Ellagic acid moieties in solution are proven to have anticarcinogenic activity towards breast cancer cells.^{24,25} They can inhibit cell proliferation as well as they help in the migration of cells through VEGF-induced angiogenesis, VEGF-2 tyrosine kinase activity (as it can interact through hydrogen bonding and aromatic interactions within the ATP-binding region of VEGFR kinase) and its downstream MAPK and PI3K/Akt pathways.^{25,26} Our results indicate that the newly synthesized TAS particles can be utilized as nanoformulations for the treatment of breast cancer cells. In addition, the TA nanoparticles can also be loaded with other antineoplastic hydrophobic drugs to enhance their therapeutic activity.

Conclusions

We have demonstrated the unexpected ability of ultrasound to perform multiple and consecutive reactions on tannin molecules. The product, *i.e.*, ellagic acid assembles and crystallizes into regularly shaped particles. The particle sizes and morphologies can be tuned by changing the ultrasonic parameters and concentration of tannic acid. We have demonstrated that the radical yield and shear forces can alter the size and morphology of the particles. TAS particles possess optical properties in a wide range of wavelengths as well as anticancer and antioxidant properties. In particular, TAS nanoparticles showed significantly higher cytotoxicity and higher radical scavenging activity as compared to that of soluble TA and EA. In conclusion, this study highlights the importance of using a powerful and green ultrasonic methodology to synthesize EA particles starting from a biomass such as TA. The synthesis was performed without using any reagents or organic solvents with a fine control over particle size and morphology. We are currently investigating the potential use of TA nanoparticles as drug delivery carriers. In addition, future efforts will be directed towards the utilization of this strategy to modify other sono-reactive molecules to obtain biofunctional molecules.

Conflicts of interest

There are no conflicts to declare.

Acknowledgements

This research was funded by the ARC Future Fellowship 2014 (project number FT140100873, to FC). S. K. B. acknowledges the University of Melbourne for the scholarships (MRS). We thank Prof. Frank Caruso for helpful discussion.

Notes and references

- 1 M. Ashokumar, *Handbook of Ultrasonics and Sonochemistry*, Springer, 2016.
- 2 M. Ashokkumar, D. Sunartio, S. Kentish, R. Mawson, L. Simons, K. Vilkh, *et al.*, *Innov Food Sci Emerg Technol.*, 2008, **9**, 155–160.
- 3 S. K. Bhangu and M. Ashokkumar, *Top. Curr. Chem.*, 2016, **374**, 56.
- 4 R. Bund and A. Pandit, *Ultrason. Sonochem.*, 2007, **14**, 143–152.
- 5 F. Cavalieri, E. Colombo, E. Nicolai, N. Rosato and M. Ashokkumar, *Mater. Horiz.*, 2016, **3**, 563–567.
- 6 S. K. Bhangu, M. Ashokkumar and F. Cavalieri, *ACS Sustainable Chem. Eng.*, 2017, **5**, 6081–6089.
- 7 L. Mingshu, Y. Kai, H. Qiang and J. Dongying, *J. Basic Microbiol.*, 2006, **46**, 68–84.
- 8 A. Brune and B. Schink, *Arch. Microbiol.*, 1992, **157**, 417–424.

- 9 Q. Sun, J. Heilmann and B. König, *Beilstein J. Org. Chem.*, 2015, **11**, 249.
- 10 S. Quideau, D. Deffieux, C. Douat-Casassus and L. Pouysegu, *Angew. Chem., Int. Ed.*, 2011, **50**, 586–621.
- 11 H. Ejima, J. J. Richardson and F. Caruso, *Nano Today*, 2017, **12**, 13.
- 12 N. Bertleff-Zieschang, M. A. Rahim, Y. Ju, J. A. Braunger, T. Suma, Y. Dai, S. Pan, F. Cavaliere and F. Caruso, *Chem. Commun.*, 2017, **53**, 1068.
- 13 E. D. Bartzoka, H. Lange, K. Thiel and C. Crestini, *ACS Sustainable Chem. Eng.*, 2016, **4**, 5194–5203.
- 14 Z. Chen, C. Wang, J. Chen and X. Li, *J. Am. Chem. Soc.*, 2013, **135**, 4179–4182.
- 15 T. Mizuno, K. Uchino, T. Toukairin, A. Tanabe, H. Nakashima, N. Yamamoto, *et al.*, *Planta Med.*, 1992, **58**, 535–539.
- 16 I. Mueller-Harvey, *Anim. Feed Sci. Technol.*, 2001, **91**, 3–20.
- 17 L. Pouységu, D. Deffieux, G. Malik, A. Natangelo and S. Quideau, *Nat. Prod. Rep.*, 2011, **28**, 853–874.
- 18 S.-J. Wu, Y.-C. Ho, S.-Z. Jiang and F.-L. Mi, *Food Funct.*, 2015, **6**, 2283–2292.
- 19 M. Z. Hussein, S. H. Al Ali, Z. Zainal and M. N. Hakim, *Int. J. Nanomed.*, 2011, **6**, 1373–1383.
- 20 S. Goriparti, M. Harish and S. Sampath, *Chem. Commun.*, 2013, **49**, 7234–7236.
- 21 M. W. Park and S. D. Yeo, *Sep. Sci. Technol.*, 2010, **45**, 1402–1410.
- 22 V. S. Nalajala and V. S. Moholkar, *Ultrason. Sonochem.*, 2011, **18**, 345–355.
- 23 S. Kaur Bhangu, M. Ashokkumar and J. Lee, *Cryst. Growth Des.*, 2016, **16**, 1934–1941.
- 24 H. M. Zhang, L. Zhao, H. Li, H. Xu, W. W. Chen and L. Tao, *Cancer Biol. Med.*, 2014, **11**, 92.
- 25 N. Wang, Z. Y. Wang, S. L. Mo, T. Y. Loo, D. M. Wang, H. B. Luo, *et al.*, *Breast Cancer Res. Treat.*, 2012, **134**, 943–955.
- 26 L. Tang, X. Ma, Q. Tian, Y. Cheng, H. Yao, Z. Liu, *et al.*, *Food Chem. Toxicol.*, 2013, **56**, 204–213.